

# Effect of Spray Particle Trajectory on the Measurement Signal of Particle Parameters Based on Thermal Radiation

Chang-Jiu Li, Tao Wu, Cheng-Xin Li, and Bo Sun

(Submitted 5 June 2001; in revised form 11 December 2001)

The influences of the dimensions of optical components and the trajectories of spray particles on the variations of the waveforms of the radiation signals from the spray particles were studied both theoretically and experimentally for correct simultaneous measurement of the particle parameters including velocity, surface temperature, size, and spatial distribution. Two types of filtering masks, including single-windowed and dual-windowed, were used as models in the current study. The evolution of the radiation pulse from a moving thermal spray particle was simulated through the change of the projected area of the particle image spot on the filtering mask window. The experimental detection of the thermal radiation pulses was performed for the high velocity oxygen fuel (HVOF) process using an optoelectronic measurement system.

The theoretical simulation clearly showed that the characteristic waveforms of the thermal radiation signals from the spray particles are varied with the distance and orientation of the trajectories of thermal spray particles with respect to the ideal image plane of the filtering window plane. The typical variations of the characteristic waveforms obtained theoretically have been observed experimentally with HVOF spraying. The waveforms expected theoretically were correlated well with those observed experimentally.

The characteristic waveforms of the radiation signals from the spray particles in a trapezoid shape with a saturated top platform contain the information for spray particle parameters including velocity, surface temperature, size, and spatial distribution. With the dual-windowed filtering mask, the particle velocity can be correctly measured with the bi-peak radiation signal in triangle-like shape, and the surface temperature may be estimated reasonably. However, the particle size cannot be estimated correctly. It was revealed that the characteristics of the waveforms were remarkably influenced by the image spot size. Therefore, the expansion of the image spot based on the relation between the image spot size of an in-flight particle and optical lens parameters obtained optically was discussed. The influence of the image spot size on the waveform characteristics was examined.

**Keywords** in-flight particle velocity, particle size, radiation pulse signal, simultaneous measurement of particle parameters, spatial aberration, spray particles, surface temperature, thermal radiation

## 1. Introduction

The properties of a thermally sprayed coating are generally influenced by a number of spraying parameters. Most important are those parameters that influence the particle condition, such as in-flight velocity, surface temperature, and particle size. Therefore, control of the particle condition parameters is essential for the optimization of coating properties and study of the coating deposition process.<sup>[1]</sup> During the late 1970s, with the development of optoelectronics, several methods based on laser velocimetry such as LDV<sup>[2]</sup> and L2V<sup>[3]</sup> were applied to measure the velocity of in-flight particles in the thermal spray process. Those methods were able to measure the in-flight particles' ve-

locity within the bright core of a plasma jet with a high accuracy. Those techniques generally required precise alignment of optical components. Moreover, it was difficult to apply those methods to a dense stream of particles under conditions for coating production.<sup>[1]</sup>

From the middle of the 1980s, a novel method to simultaneously measure particle temperature, velocity, and size using an optical diagnostic technique was proposed.<sup>[4,5]</sup> This method was based on the detection of thermal radiation emitted by the in-flight particles at a high temperature. Based on the work of Moreau et al., the commercially available particle condition monitoring system, the DPV-2000 system (Tecnar Automation, QC, Canada), was developed.<sup>[6]</sup> During the measurement of spray particle parameters, a well-separated bi-peak pulse was selected for the evolution of particle parameters that corresponds to the particle passing near the focal plane; other types of signals were not taken into consideration and were completely neglected.<sup>[6]</sup> With this selection of signals, only the signal from particles near the focal plane were sorted out, which yielded particle velocity with good accuracy and surface temperature with reasonable accuracy assisted by the calibration. Therefore, the system has been applied more widely to the measurement of particle condition parameters from plasma spraying,<sup>[7-13]</sup> HVOF,<sup>[14-17]</sup> and the arc spraying process.<sup>[18]</sup> Practically, vari-

Chang-Jiu Li, Tao Wu, Cheng-Xin Li, and Bo Sun, Welding Research Institute, School of Materials Science and Engineering, Xi'an Jiaotong University, Xi'an, Shaanxi, 710049, P.R. China. Contact e-mail: licj@mail.xjtu.edu.cn.

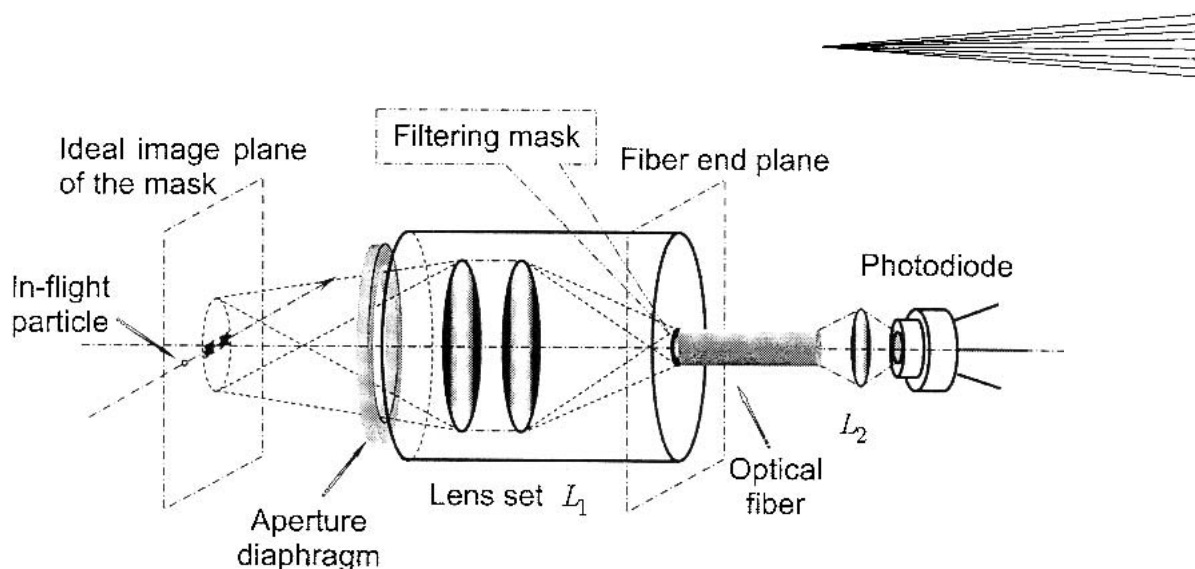


Fig. 1 Schematic diagram of the setup of the optical components in the measurement system

ous types of pulses, from a well-separated one to a considerably superimposed pulse, are detected during measurement.

A system based on a principle similar to DPV-2000 with more rapid evolution of particle parameters aiming at on-line control of the spray process was recently developed.<sup>[19]</sup> Another recent investigation illustrated that an offset of in-flight particle trajectory from the focal plane not only results in the decrease in magnitude of the signal, but also in the variation of the signal's waveform from a rectangular shape to a triangle-like one.<sup>[20]</sup> The result implies that the selection of a valid signal may influence measurement accuracy of particle parameters, especially with the measurement of particle size. This is because the magnitude of the signal from a particle at the same condition may be changed owing to the change of trajectory with respect to focal plane. But the particle size is determined by the magnitude of the signal detected from a spray particle. However, up to now, there has been a lack of theoretically comprehensive analysis of pulse signal evolution, subsequent pulse configuration, and variations of pulse waveform. The current study into the evolution of the pulse waveforms emitted by thermal spray particles revealed that the pulse waveforms could be altered by the design of an optical system and the spatial trajectory of the spray particle in the measurement region. Consequently, variations of the pulse waveform occur, which significantly influence the evolution of particle parameters.

Here we describe a model system comprised of single or dual transparent window filtering masks with dual color-filtering channels. The system was used for the detailed theoretical analysis of the evolution of the optoelectronic signal waveforms and experimental investigation to clarify the factors that influence the evolution of particle parameters through thermal radiation.

## 2. A Theoretical Model of the Radiation Signal by a Thermal Spray Particle

### 2.1 The Optical Model

The general setup of the optical sensor head in the measurement system is depicted in Figure 1. A filtering technique was

used to obtain optoelectronic pulse signals associated with particle movement. The optical sensor head consisted of an aperture diaphragm, a set of lens  $L_1$ , and a filtering mask placed onto the front-end plane of a transmitting optical fiber. The effective incident diameter of the fiber was 2 mm. Two types of square transparent windows were used as a filter mask; the first with one window and the other with two windows, as shown in Fig. 2(a) and (b), respectively.

Figure 3 schematically shows the geometrical relation between the lens set  $L_1$  inside the optical sensor head and spraying jet. Based on the principles of geometrical optics, the filtering mask plane in the sensor head will form an image plane outside the sensor head. When the radiation from a hot in-flight particle carried by a jet is transmitted through the optical lens set  $L_1$ , it will form a corresponding image spot at the plane where the filtering mask was placed. Through the modulation by the window(s) on the filtering mask, the movement of such an image spot is converted into an optical pulse signal.

Since the size of the spray powder is smaller than 200  $\mu\text{m}$  in diameter, an individual particle can be considered as a dot-sized lamp-house. Therefore, its image can be considered as an image spot. On the other hand, the depth of the focus of the lens set leads to the spatial expansion of the image of the filtering mask as shown in Fig. 3. Moreover, most particles will randomly pass through the expanded image area of the filtering mask rather than the theoretical image plane. This implies that the positions of the image spots of most spray particles will be apart from the ideal filtering mask plane at the direction of primary axis of the optical lens set. The intersected area of the radiation beams from the image spots and the plane of filtering mask present a series of "ellipse" zones. Because the offset of the image spot to the mask plane and the diameter of filtering mask are much smaller than the distance from the optical center of the lens set to the mask plane, the length of the long axis of the "ellipse" is approximately equal to the length of the short axis. It can thus be considered as a circular zone.

When a particle passes through the measurement zone and the radiation from the particle passes through this circular area, a pulse of light intensity will appear behind the filtering mask,

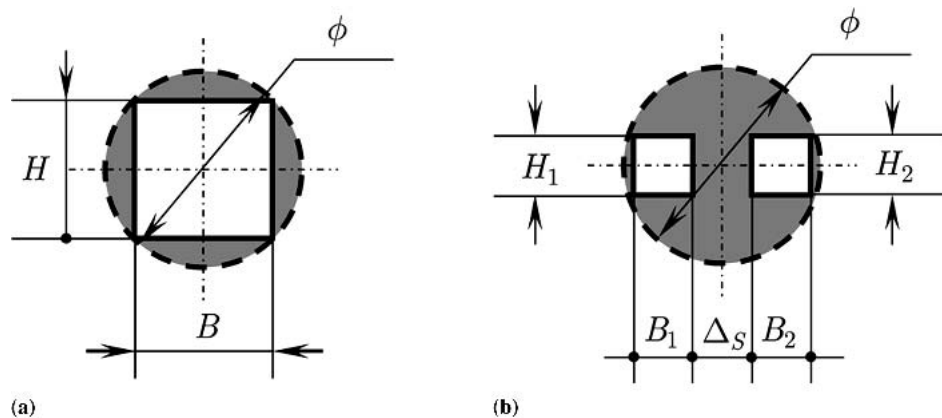


Fig. 2 Schematic diagram of the models of filtering window: (a) single-window model, (b) dual-window model

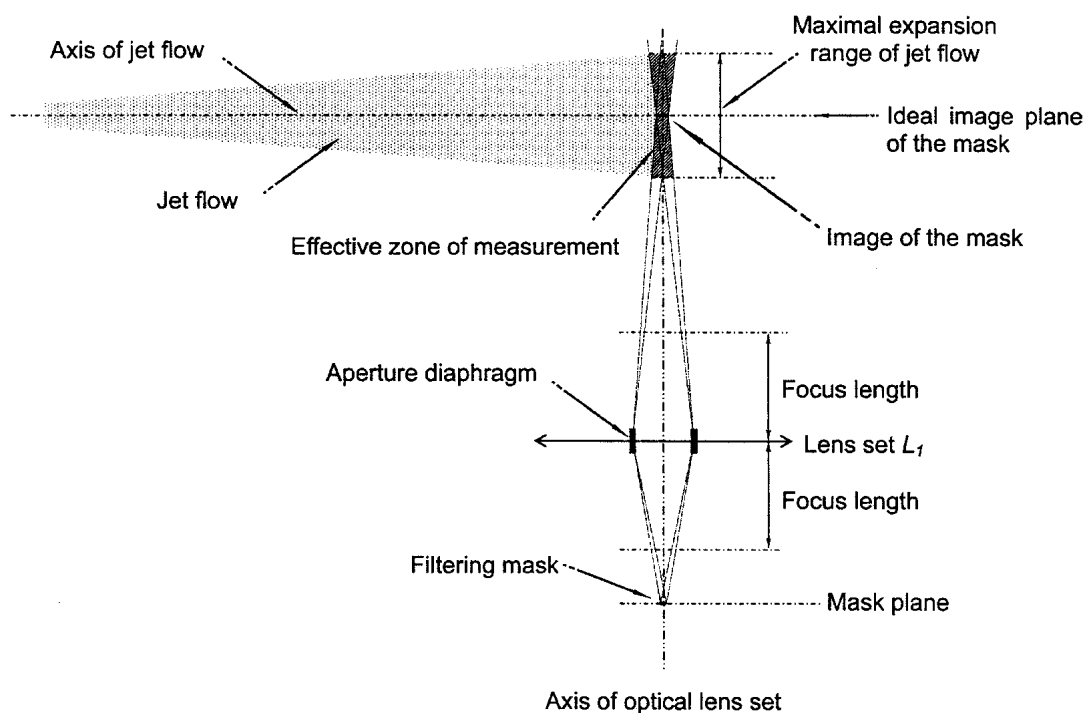


Fig. 3 Schematic diagram of the effective flame zone where the radiation can reach to the filtering mask from the in-flight particle

with time. However, only the particles passed through the image plane of the filtering mask correspond to the theoretical image spot size on the filter mask. The image spot on the filter mask from other particles, without passing along the image plane, corresponds to an expanded spot. Such a spot carries the maximal effective thermal radiation energy that can be transmitted to the mask plane by the lens set, due to the limitation of the aperture diaphragm. The expansion of the image spot will influence the characteristics of the waveform of the modulated pulse signal.

## 2.2 The Radiation Signal by a Single-Window Filter Model

For the radiation of a hot particle, it can be reasonably supposed that the thermal radiation energy from the dot-sized lamp-

house is uniformly distributed on the image spot expanded on the filtering mask. Compared with the distance from the particle to the front-end of the lens set, the offset of the particle from the image plane of the filtering mask is quite small, which does not remarkably change the thermal radiation energy from the particle entering the lens set. Consequently, the intensity of the subsequent radiation pulse modulated by the window will be proportional to the projected area of the image spot on the masking window, as shown by Fig. 4. As a result, the final intensity of the pulse signal converted optoelectronically from the original optical pulse must be proportional to the projected area of the image spot on the masking window. Therefore, the evolution of the radiation pulse from the spray particle can be theoretically simulated through the change of the projected geometrical area of the

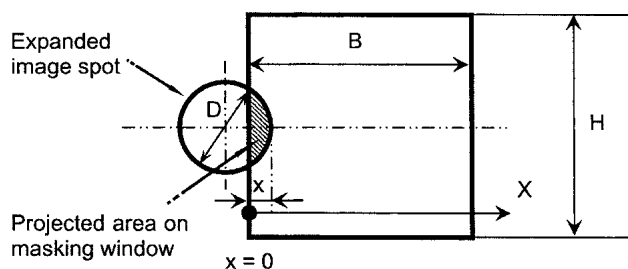


**Fig. 4** Schematic diagram of the projecting effect of an expanded image spot corresponding to the evolution of radiation pulse signal with the single-window filtering mask

expanded image spot on the masking window against the displacement along the  $x$  axis as shown in Fig. 4. For the comparison, intensity of the pulse peak was normalized using a maximum spot area in the following simulating calculation.

Supposing that  $H$  and  $B$  are the height and width of the transparent window on the mask, respectively, and  $H$  is much larger than the diameter of the light image spot  $D_s$ , the variations of pulse signals can be divided into four types depending on the relative ratio of  $B$  to  $D_s$ . Those four types correspond to the following conditions:

Type I:  $D_s < B$

Type II:  $B = D_s$


Type III:  $D_s/2 < B < D_s$

Type IV:  $B < D_s/2$

Using the maximum projected area in each case mentioned above as an indication of corresponding maximum intensity to normalize the pulse signal, the characteristic waveforms representing the pulse signals in each type can be expressed as shown in Fig. 5.  $S_{s_{max}}$  and  $S_{max}$  represent the total effective radiation and the maximum radiation in each type. It can be found that the four types of signals show different characteristic waveforms. Type I and Type II are referred to as a curve-sided trapezoid and a curve-sided triangle, respectively. Type III and Type IV are referred to a rounded hill shape.

With a Type I signal, when the image spot enters the window area, with an increasing exposure of the spot in the window, the intensity of radiation from the particle becomes strong gradually. After the spot fully enters into the masking window, the whole effective radiation of the particle passes through the window and the most intense radiation is obtained. This maximum will be maintained at a saturated level ( $S_{s_{max}}$ ) until the image spot reaches the other side of the masking window. With a Type II signal, as soon as the spot enters the window area and the intensity of the pulse reaches the maximum  $S_{s_{max}}$ , it reaches to the other side of the window wall. Therefore, a symmetrical triangle-like pulse is formed.

With Type I and Type II pulse signals, the half-width at full maximum (HWFM) of the signal peak corresponds to the width of the transparent window on the filtering mask. The maximum level of the pulse is proportional to the radiation from all of the effective surface area of the spray particle. Therefore, the particle velocity, surface temperature, and particle size are directly related to the HWFM, and the maximum height of the pulse, respectively. Moreover, it is evident that Type II is an ultimate case of Type I.



With Type III and Type IV pulse signals, as shown in Fig. 5(c) and (d), the HWFM of the pulse signal becomes larger than the width of the masking window and the maximum of the pulse becomes less than the maximum ( $S_{s_{max}}$ ), which is proportional to the effective surface area. Therefore, the current maximum radiation does not contain information of particle size and the HWFM is not associated directly with the particle velocity. On the other hand, the full width of the pulse at ground level corresponds to the width of the masking window plus the diameter of the image spot. However, it is rather difficult to obtain the characteristic values practically, such as the total width of those peaks at ground level, due to the background noise involved in practically signal. As a result, it is difficult to obtain particle velocity and impossible to obtain the particle size with those types of pulse signals. Therefore, when a single transparent window-filtering mask is used, it is necessary to use a window with a width larger than the image spot size of the particles.

### 2.3 The Radiation Signal by a Dual-Window Filter Model

With a dual-window filter, besides the effect of the relative ratio of the width of the window to the image spot size on the variations of pulse signals similar to the single-window model, the interval ( $\Delta_s$ ) between two windows relative to the image spot size ( $D_s$ ) also has a significant effect on the characteristics of the waveforms of the pulse signal. Figure 6 shows a model of a dual-window filter for the investigation of the variations of signal pulse waveforms. For simplicity, the calculation was performed for typical combinations of the masking windows' dimensions and the image spot sizes.

Figures 7-9 depict the effects of  $\Delta_s$  and  $D_s$  on the simulated waveforms of the pulse signals under different masking windows' dimensions. It can be found that when the interval is larger than the image spot size, a couple of separated curve-sided trapezoid pulse signals are formed. With the decrease in the interval to less than  $D_s$ , as shown in the first columns in Fig. 7-9, the dual peaks approach close gradually, to become overlapped. The degree of such overlapping becomes more remarkable as  $\Delta_s$  becomes much less than  $D_s$ . In the ultimate case of  $\Delta_s = 0$ , the dual peak becomes one single peak. On the other hand, with the increase in the image spot size, the fraction of the projected area of the spot size on the window relative to the whole spot size is decreased. This means that the effective radiation from the spray particle will be decreased. Moreover, the overlapping of the dual peak occurs at a larger window interval. Consequently, the various pulse signals in various waveforms can be obtained. Figures 8 and 9 show the effect of the interval of dual-window on the waveforms of pulse signals under the condition of  $B < D_s/2$ . All pulse signals give a maximum much less than the saturated level of effective radiation corresponding to the area of the image spot. The effect of the overlapping on the patterns of the waveforms becomes more remarkable. Comparing signals in Fig. 9 with those in Fig. 8, it is clear that the height of the windows mainly influences the overall level of the signal when the image size becomes larger than the height.

Therefore, it is clear that with the dual-window filtering mask, the dimension of transparent windows ( $B_1, H_1, B_2, H_2$ ) and the window interval will significantly influence the subsequent waveforms of the pulse signals. The effects of those pa-

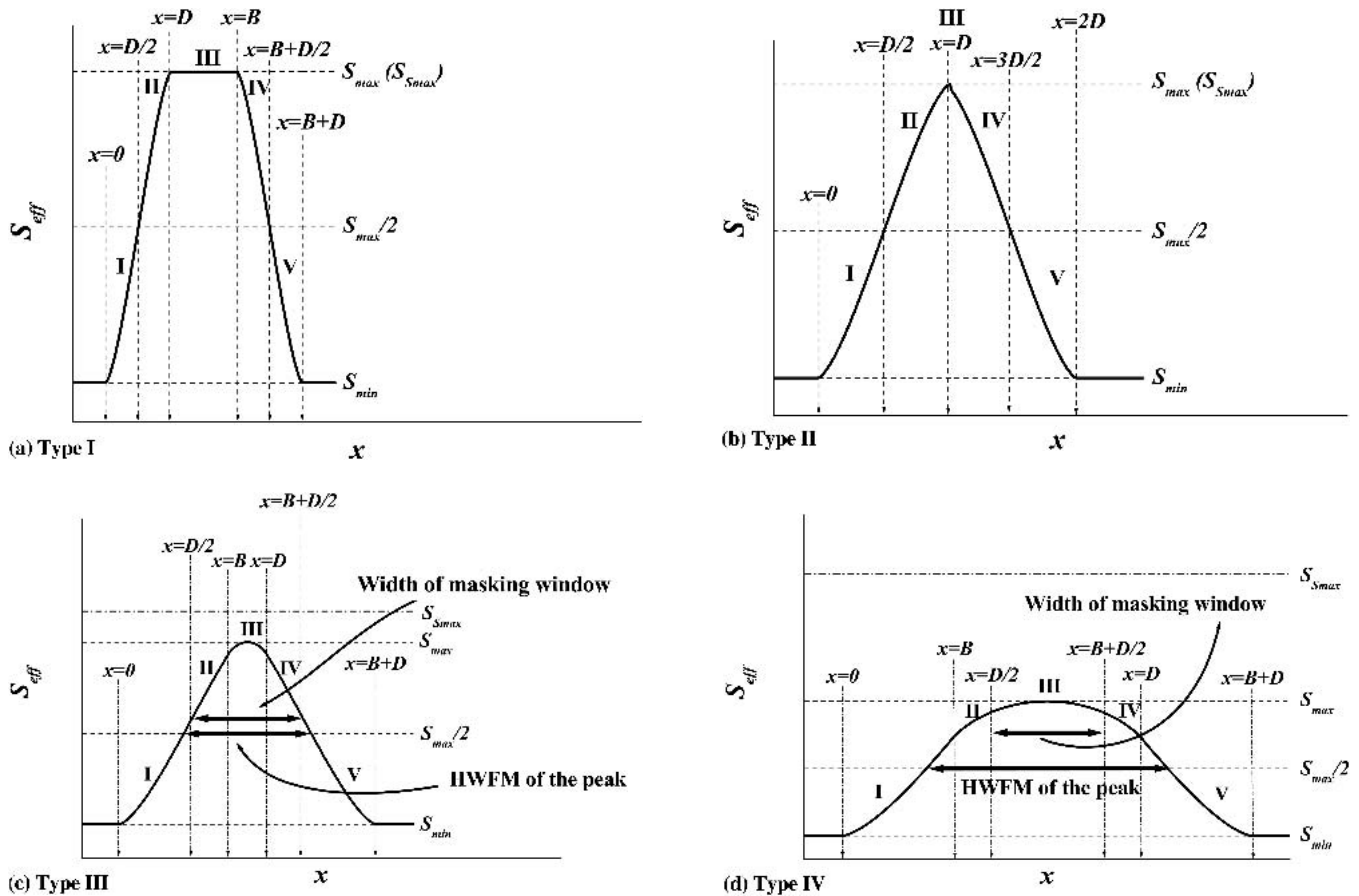


Fig. 5 Schematic illustration of typical waveforms of four types of radiation signals: (a) Type I:  $B > D_s$ ; (b) Type II:  $B = D_s$ ; (c) Type III:  $D_s > B$ ; (d) Type IV:  $B < D_s/2$

parameters should be taken into consideration during the design of the windowed filtering mask to obtain near dual trapezoid-shaped peaks.

### 3. The Effect of the Particle Offset From the Theoretical Mask Image Plane on the Expansion of the Image Spot

The previous results clearly show that the image spot size has significant influence on the resulting waveforms of the pulse signals. When the image spot size expands to over the interval between the windows, overlapping of the dual peaks becomes significant. Such overlapping will make the extraction of useful information from the waveform pattern difficult. Regarding the expansion of the image spot, as shown in Fig. 10, there are two factors that influence the size of the expanded image spot. Those factors are the offset of particle position to the ideal mask image plane along the axis of the optical lens set and the effective optical aperture of the lens set.

In the spatial zone where the radiation from the particle can be transmitted partially or entirely to the mask, when the trajectory of an in-flight particle is not in the ideal image plane of the mask, field aberration will occur. As a result, the image spot will be expanded on the mask plane independent of spray particle

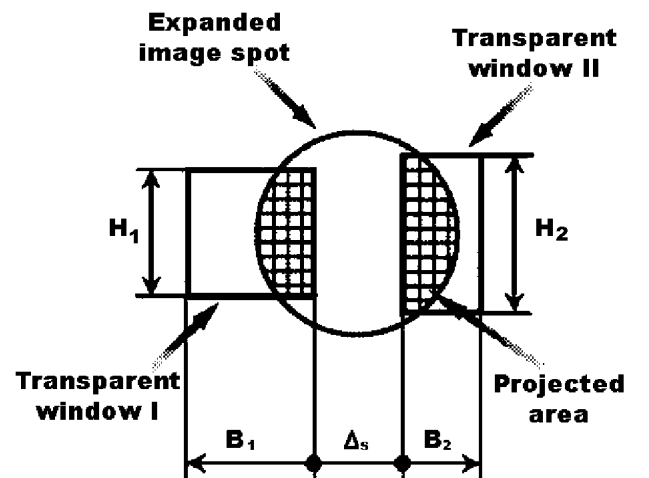
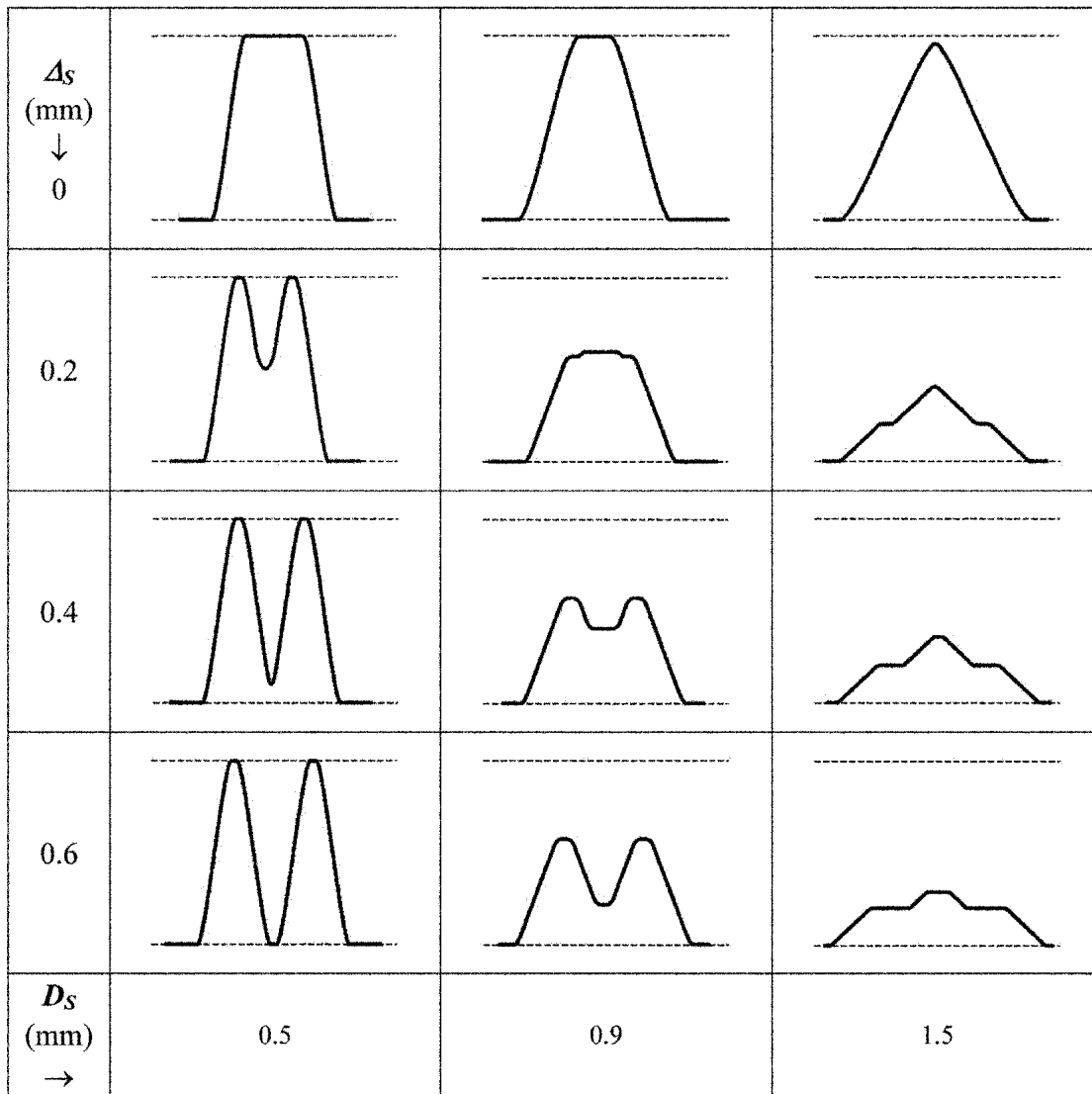


Fig. 6 Schematic diagram of the projecting effect of an expanded image spot corresponding to the evolution of radiation pulse signal with the dual-window filtering mask

size. The radiation from the spray particle will be transmitted onto the mask plane through an expanded image spot zone instead of an ideal image spot of spray particle.

Under this condition, the diameter of the expanded image



**Fig. 7** Effects of  $\Delta_s$  and  $D_s$  on the simulated waveforms of the pulse signals. The signals in the top row were calculated for single-window filtering mask under  $B = H = 1.4$  mm. All other signals were for dual-window filtering mask under  $B_1 = H_1 = B_2 = H_2 = 0.6$  mm

spot of the particle can be derived optically as the functions of the offset ( $\Delta x$ ) and the effective aperture ( $D$ ) as follows:

When  $\Delta x > 0$ ,

$$D_s = D \cdot \frac{x'_0 \cdot \Delta x}{(f + x'_0)(x_0 + \Delta x) - x'_0 \cdot \Delta x} \quad (\text{Eq 1})$$

When  $\Delta x < 0$ ,

$$D_s = D \cdot \frac{-x'_0 \cdot \Delta x}{(f + x'_0)(x_0 + \Delta x) - x'_0 \cdot \Delta x} \quad (\text{Eq 2})$$

where  $f$  is the focus length of the main lens set,  $x_0$  the object distance, and  $x'_0$  the image distance, respectively. In the present system,  $D, f, x_0$ , and  $x'_0$  were set to 20 mm, 35 mm, 70 mm, and 17.5 mm, respectively. Under these geometrical conditions, the

effects of the offset and effective aperture on the diameter of the expanded image spot were estimated.

Figures 11 and 12 show the variations of  $D_s$  with the effective aperture and offset of the particle under both  $\Delta x > 0$  and  $\Delta x < 0$ , respectively. The  $D_s$  was plotted as lines of equivalence.

From the above results, the diameter of the expanded image spot is determined from the combination of the offset and the effective aperture. It can also be recognized that the expansion of the image spot is more remarkable under the condition  $\Delta x < 0$  compared with that under  $\Delta x > 0$ .

Under the condition  $\Delta x > 0$ , when the offset is given a value of 20 mm and the dual-window filtering mask shown in Fig. 2(b) is used, the effective aperture of the lens set should be controlled below 7.4 mm to ensure that the diameter of the expanded image spot is smaller than the width of the masking window. When a single-window mask is used, the diameter should be controlled below 16.8 mm. On the other hand, under the condition  $\Delta x < 0$ ,

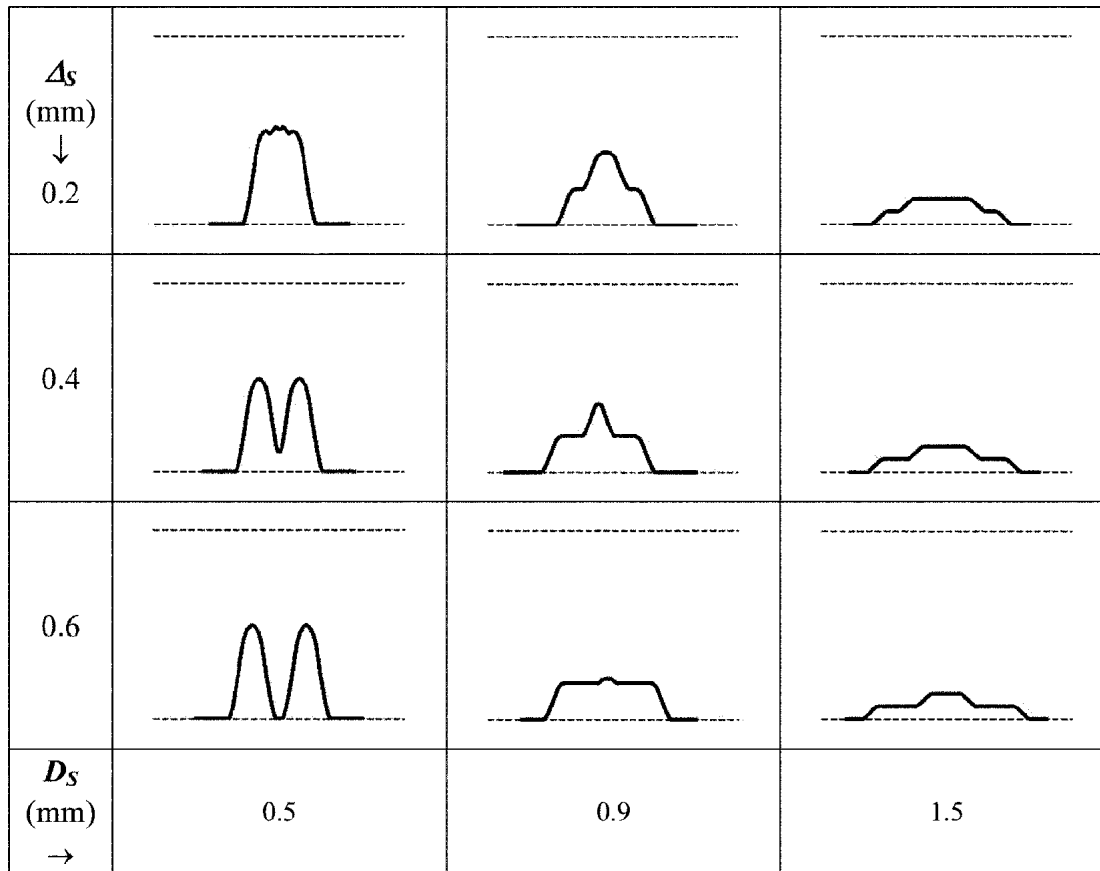


Fig. 8 Effects of  $\Delta_s$  and  $D_s$  on the simulated waveforms of the pulse signals under  $B_1 = B_2 = 0.2$  mm and  $H_1 = H_2 = 0.6$  mm

the apertures for dual-window and single window masks are required to be less than 5.1 mm and 11.2 mm, respectively.

However, it should be noted that the total intensity of the radiation, which can pass through the lens and reach the mask plane, is proportional to the square of the effective aperture. The decrease of the effective aperture will result in a significant decay of the intensity of the radiation from the hot in-flight particle. For the practical optical system, the selection of an aperture large enough to ensure the intensity of the radiation signal is necessary.

#### 4. The Effect of Spatial Distribution of Particles on the Characteristics of Radiation Signals

The previous results clearly show that the offset of particles from the ideal mask image plane leads to significant expansion of the image spot on the mask plane. The degree of the expansion is increased with the increase in the offset. On the other hand, this expansion leads to the variations of the waveforms of the radiation signals. Because an in-flight particle may travel with a certain angle to the axis of the flame jet, the offset of the particle may vary during its passing through the effective measurement zone. Therefore, it is necessary to study the effect of particle trajectories on the expansion of the image spot and subsequently

on the waveforms of the radiation signal. Figure 13 schematically shows the spatial zone that spray particles pass through during HVOF spraying. To reveal the significance of the influence, the following four cases were considered. In all cases the trajectory of a spray particle is regarded as a straight line. The effective projected area of the image spot on the masking window is still taken as an indication of the radiation intensity from the spray particle.

- 1) Case I. The trajectory of a spray particle is parallel to the torch axis  $y$ , and the particle only has an offset. Such an offset will influence the subsequent waveforms of the radiation signals through the expansion of the image spot size.
- 2) Case II. The trajectory of the particle is in the plane parallel to the  $yo$ z plane and is inclined by an angle ( $\alpha$ ) to the  $xo$ z plane. In this case, the offset of the particle  $\Delta x$  is still a fixed value, but its vertical position varies with distance due to the inclination of the particle trajectory with the  $xo$ z plane. From most HVOF conditions, it was estimated experimentally that  $\alpha$  is generally less than  $6.8^\circ$  with the HVOF system used in the current study.
- 3) Case III. The trajectory of the particle is in the plane parallel to the  $xo$ z plane and inclined by an angle ( $\beta$ ) to the  $yo$ z plane. In this case, the offset of the particle is varied with traveling owing to the inclination of the trajectory to the  $yo$ z plane. The angle  $\beta$  was also generally less than  $6.8^\circ$ .

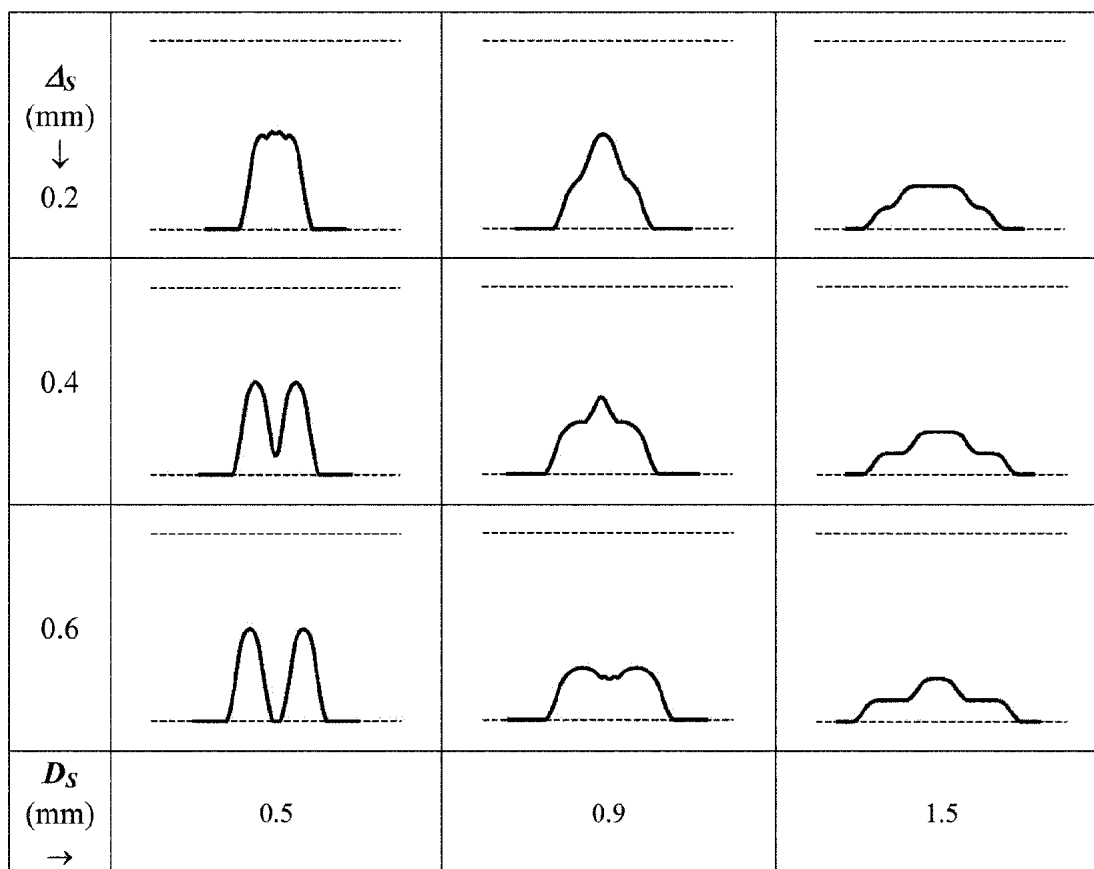


Fig. 9 Effects of  $\Delta s$  and  $D_s$  on the simulated waveforms of the pulse signals under  $B_1 = B_2 = 0.2$  mm and  $H_1 = H_2 = 1.0$  mm

- 4) Case IV. The trajectory of the particle is an arbitrary straight line inside the cone of jet flow. This condition can be considered as the superimposition of the Cases (2) and (3).

#### 4.1 Asymmetrical Deformation of the Signal Peaks by a Single-Window Filter Model

Using a single-window filtering mask as shown in Fig. 2(a), the variations of the pulse signal from the radiation of the spray particle were simulated for the above mentioned Cases 2, 3, and 4. Figure 14 shows the typical results for each case.

From these results, it can be found that the characteristic signal peaks in the trapezoid shape are deformed due to the inclinations of particle trajectory to the torch axis. It is clear that the inclination  $\alpha$  mainly causes the deformation of the height of the trapezoid peak for the particle, the image of which is partially shielded owing to the encounter of the image spot with the top or bottom border of the masking window. The inclination  $\beta$  will cause an asymmetrical elongation of the signal. Those results indicate that the pulse signal from the radiation in the trapezoid shape will experience certain deformation owing to the arbitrary trajectory of the spray particle in the flame jet.

Based on the estimated values of  $\alpha_{\max}$  and  $\beta_{\max}$  for the present HVOF flame jet mentioned previously, the deformation will not significantly affect the extraction of the characteristic

parameters from the radiation signal for the estimation of particle parameters. However, for a particle stream with a large divergent angle, such an effect would be significant for the determination of particle parameters.

#### 4.2 Asymmetrical Deformation of the Signal Peaks by Dual-Window Filter Model

With the dual-window filtering mask as shown in Fig. 2(b), when both the width and height of each window and the interval gap between the two windows were set to 0.6 mm, the typical waveforms of the radiation signals obtained by numerical simulation are shown in Fig. 15 to correspond to the three different cases.

It is clear that the asymmetrical deformation of the signal waveforms occurs more significantly owing to the inclination of the particle trajectory to the axis of the flame jet. The waveform of the second peak in the bi-peak signal becomes more dissimilar to the first one. This asymmetrical deformation of the peaks causes the difficulty to determine characteristic peak parameters and leads to the occurrence of a serious error in the determination of spray particle parameters. Compared with the deformation of the radiation signal with the dual-window filtering mask, the deformation of the radiation signal obtained by the single-window filtering mask is reasonably tolerated under the conditions in the current study.



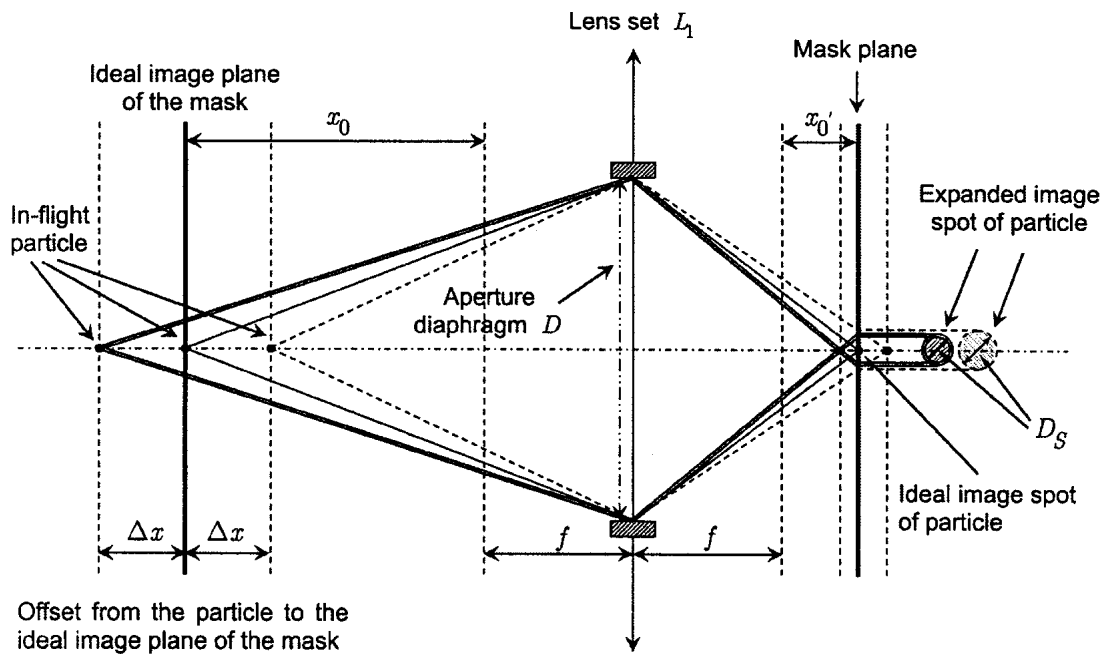


Fig. 10 Schematic illustration of the expansion of the image spot of a particle

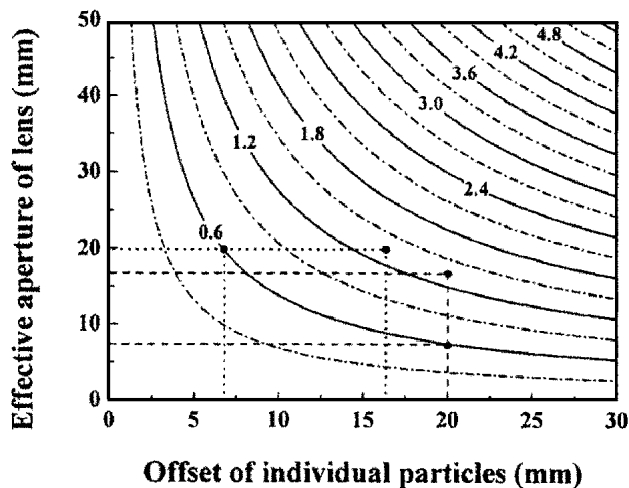


Fig. 11 Effects of offset  $\Delta x$  and effective aperture  $D$  on the diameter of expanded image spot  $D_s$  under the condition  $\Delta x > 0$  (unit: mm)

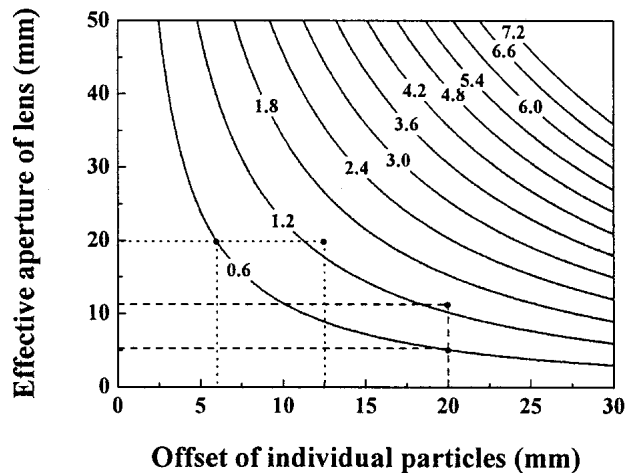


Fig. 12 Effects of offset  $\Delta x$  and effective aperture  $D$  on the diameter of expanded image spot  $D_s$  under the condition  $\Delta x < 0$  (unit: mm)

## 5. Experimental Correlations

### 5.1 System Set-Up

Figure 16 schematically shows the setup of the integrated system for the experiment. The distance from the theoretical image plane of the mask plane to the front end of the optical sensor head was 70 mm, following the optical lens system design to protect the optical sensor from the effect of the hot jet plume. The light beam emitted by the in-flight particle was projected on the mask plane by the optical lens set. Subsequently, an image spot of the particle was formed on the mask plane. After being filtered by the transparent window(s), the light beam was guided

along an optical fiber and split into two light beams of equal radiation intensity by a half-mirror. Two beams were filtered by two monochromatic filters with  $650 \pm 5$  nm and  $770 \pm 5$  nm pass bands, respectively. The two beams were then transmitted by two optical fibers into two channels of optoelectronic conversion/preamplification modules with the same electronic parameters. The photosensitivity can be adjusted by an adjustable pre-amplifier in three gain levels: 30, 300, and 3000 mV/ $\mu$ W. Subsequently, electric pulse signals with a magnitude of  $\pm(100 \sim 999)$  mV were output by two channels. The signals were recorded by a personal computer through an Industry Standard Architecture (ISA) bus sampling card. The acceptable signal voltage level of the sampling card is  $\pm 1$  V, and the maximum

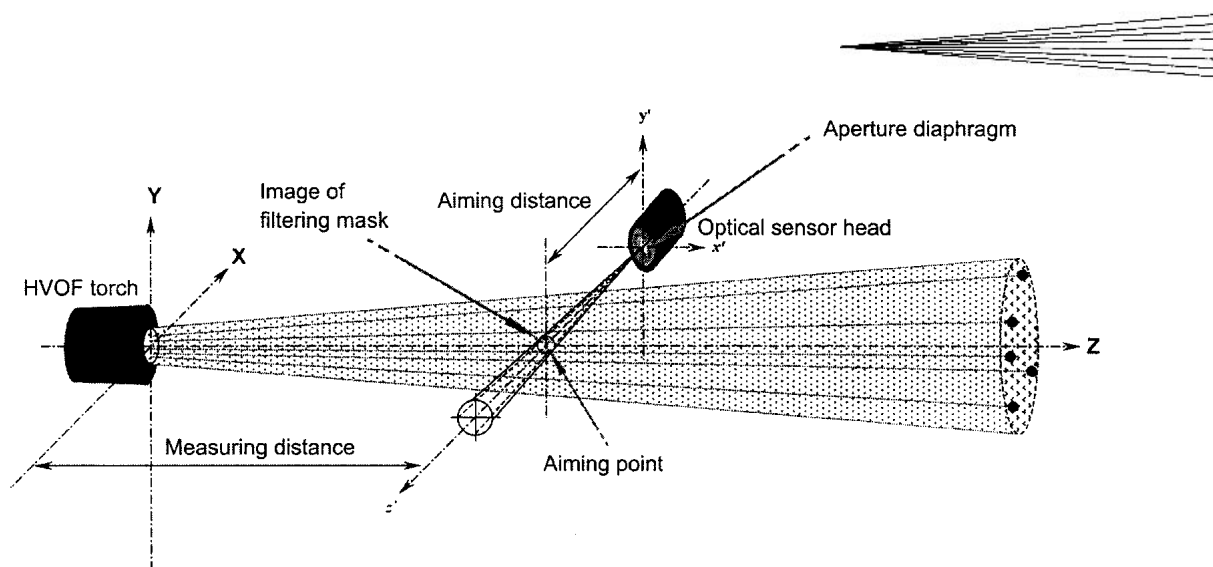


Fig. 13 Schematic illustration of the spatial zone where thermal spray particles pass in straight trajectories

sampling frequency of the card was 30 MHz. Because there were four basic frequency clock options (30, 20, 2, and 0.2 MHz) and four frequency divider options (1, 2, 4, and 8), an appropriate working mode of the sampling board could be easily accommodated.

## 5.2 The Determination of Particle Parameters From the Thermal Radiation Signals

**5.2.1 The Particle Velocity.** With the present system, the time ( $t$ ) for an in-flight particle to pass through the image area of the filtering windows in the image plane of the mask is equal to the time for the particle's imaging spot to pass through the real transparent windows on the mask plane. The moving speed of the image spot of a particle and the actual moving velocity of the particle fulfill the optical leverage relationship. This yields the expression  $v_p/l_i = v_i/l_0 = t$ , where  $l_i$  is the characteristic length of the image of filtering mask,  $l_0$  the characteristic length of the real masking window,  $v_p$  and  $v_i$  the particle velocity and image spot moving speed on the filtering mask plane, respectively. With the single-window filtering mask,  $l_0$  is actually the width of the transparent window; while with a dual-window mask,  $l_0$  corresponds to the interval between the centers of two windows. Under an ideal imaging situation,  $l_i/l_0 = M_0$ , where  $M_0$  is the magnification of the optical lens set. Therefore, the following equation can be used to calculate the particle velocity:

$$v_p = M_0 \cdot v_i \quad (\text{Eq 3})$$

when the image spot of an in-flight particle moves on the mask plane, the intensity of light radiation from the particle is modulated into a pulse signal through masking window(s) as shown in Fig. 17. From such pulse signals, the characteristic time can be obtained and the velocity of image spot  $v_i$ , and subsequently, particle velocity  $v_p$  can be calculated.

**5.2.2 The Surface Temperature.** The surface temperature of the in-flight particle is obtained by using the technique of two-color pyrometry with two monochromatic radiations from two-color filtering channels as shown in Fig. 16. The radiation

intensity from an objective is the function of its temperature and the wavelength of the radiation. The ratio of the radiation intensity at two different wavelengths can be expressed as follows:

$$R_E = \frac{E_{b\lambda_1}}{E_{b\lambda_2}} = \frac{\varepsilon_{\lambda_1}}{\varepsilon_{\lambda_2}} \cdot \left(\frac{\lambda_2}{\lambda_1}\right)^5 \cdot e^{\frac{c_2}{T} \cdot \left(\frac{1}{\lambda_2} - \frac{1}{\lambda_1}\right)} \quad (\text{Eq 4})$$

If two close wavelengths  $\lambda_1$  and  $\lambda_2$  of the two-color filters are properly chosen, the ratio of  $\varepsilon_{\lambda_1}/\varepsilon_{\lambda_2}$  is reasonably equal to the unit. As a result, the particle temperature is related to the ratio of radiances as follows:<sup>[21]</sup>

$$T_r = c_2 \cdot \left(\frac{1}{\lambda_2} - \frac{1}{\lambda_1}\right) \cdot \left[\ln R_E - 5 \ln \left(\frac{\lambda_2}{\lambda_1}\right)\right]^{-1} \quad (\text{Eq 5})$$

Here  $T_r$  is defined as the two-color radiation ratio temperature, where  $c_2$  is the second radiation constant of Planck's Law.

**5.2.3 The Particle Size.** According to the Stefan-Boltzmann's law,<sup>[22]</sup> the total radiation per unit area from a gray body ( $E$ ) at temperature ( $T$ ) can be expressed as follows:

$$E = \varepsilon \cdot E_b = \varepsilon \cdot \sigma \cdot T^4 \quad (\text{Eq 6})$$

where  $\varepsilon$  is the blackness coefficient of a gray body and  $\sigma$  is the Stefan-Boltzmann's constant.

From the shielding effect of the filtering mask to the expanded image spot discussed previously, when the diameter of the expanded image spot is smaller than the width of the filtering window, the waveform from the radiation signals will take the shape of a curve-sided trapezoid. Ideally, the top of the trapezoid forms a platform and reaches to a maximal "saturated" level that is proportional to the radiation from the whole effective particle surface. With a spherical spray particle, the saturated maximum level of the radiation signal  $E_{\max}$  can be expressed as follows in diameter  $d_p$ :

$$E_{\max} \propto d_p^2 \cdot T^4 \quad (\text{Eq 7})$$

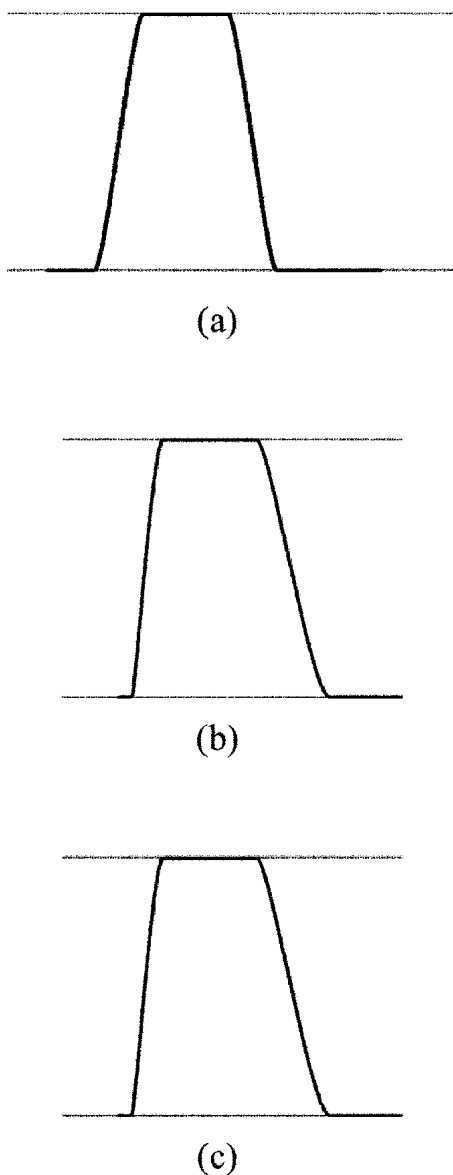


**Fig. 14** Numerical simulation results for the radiation signals of in-flight particles in the different trajectories with the single-window filtering mask: **(a)** Case II:  $a = 7.5^\circ$ ,  $B = 0^\circ$ ,  $D_s = 0.5$  mm,  $B = 1.4$  mm,  $H = 1.4$  mm; **(b)** Case III:  $a = 0^\circ$ ,  $B = 7.5^\circ$ ,  $D_s = 0.5$  mm,  $B = 1.4$  mm,  $H = 1.4$  mm; **(c)** Case IV:  $a = 7.5^\circ$ ,  $B = 7.5^\circ$ ,  $D_s = 0.5$  mm,  $B = 1.4$  mm,  $H = 1.4$  mm

This gives

$$d_p = K \cdot E_{\max}^{1/2} \cdot T^{-2} \quad (\text{Eq 8})$$

where  $k$  is a constant related to the setting of the measurement system. It should be noted that the above relation is valid only for the particles that their images completely enter the filtering window. Otherwise, the maximum intensity of the radiation peak from the particle is not proportional to the radiation from the whole particle effective surface, and Eq 8 becomes invalid.

**5.2.4 The Offset of the Particle to the Ideal Image Plane of the Filtering Mask.** When the diameter of the expanded im-

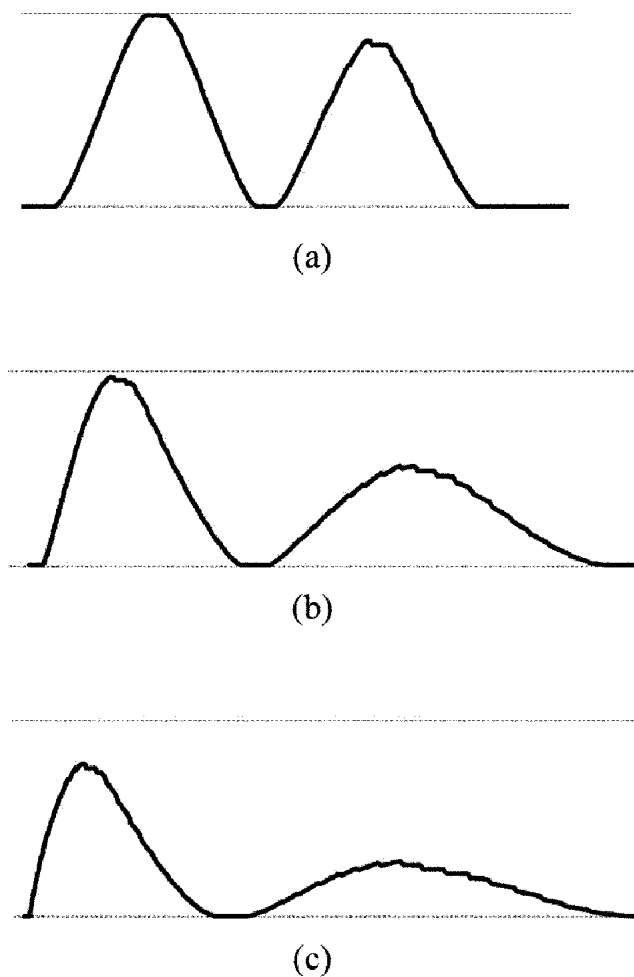


**Fig. 15** Numerical simulation results for the radiation signals of in-flight particles in the different trajectories with the dual-window filtering mask: **(a)** Case II:  $a = 7.5^\circ$ ,  $B = 0^\circ$ ,  $D_s = 0.5$  mm,  $B_1 = H_1 = B_2 = H_2 = 0.6$  mm,  $D_s = 0.6$  mm; **(b)** Case III:  $a = 0^\circ$ ,  $B = 7.5^\circ$ ,  $D_s = 0.5$  mm,  $B_1 = H_1 = B_2 = H_2 = 0.6$  mm,  $D_s = 0.6$  mm; **(c)** Case IV:  $a = 7.5^\circ$ ,  $B = 7.5^\circ$ ,  $D_s = 0.5$  mm,  $B_1 = H_1 = B_2 = H_2 = 0.6$  mm,  $D_s = 0.6$  mm

age spot is smaller than the width of the single-filtering window by an appropriate selection of the effective aperture, a trapezoid-shaped pulse peak can be observed as the Type I shown in Fig. 5(a). The ascending time or the descending time of this peak can be easily measured; it corresponds to the time that the expanded image spot accomplishes a displacement of  $D_s$ . Thereafter, the  $D_s$  can be obtained by particle velocity. According to Eq 1 and 2 or the results shown in Fig. 11 and 12, the offset can be estimated when the image plane of the filtering mask is controlled to fulfill the condition  $\Delta x < 0$  or  $\Delta x > 0$ . With the offsets of spray particles, the spatial distribution of the spray particle can be estimated if the ideal image plane of the filtering mask is placed at one boundary of the flame jet.

### 5.3 Experimental Correlation

To correlate the theoretical simulation results with the experiment, the practical detection of the radiation signals was performed using the system setup shown in Fig. 16, with both the

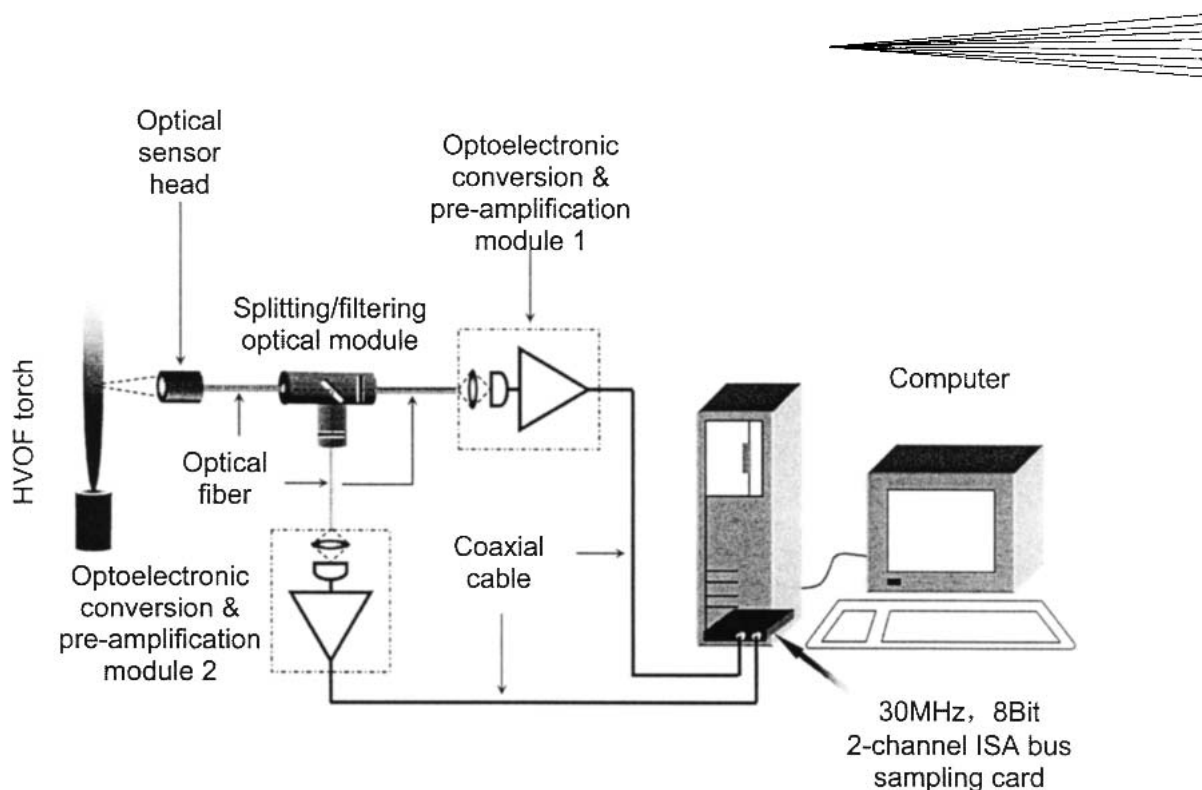


Fig. 16 Schematic diagram of the system set-up for the detection of the radiation signal from thermal spray in-flight particle

single-window and dual-window filtering masks as shown in Fig. 2. The measurement was performed with the HVOF spraying process (CH-2000 Model, Xi'an Jiaotong University, Xi'an, China). Table 1 shows the typical experimental conditions. W-20Ni powder with a 10 ~ 44  $\mu\text{m}$  particle size was used in the experiment as a model material.

Figure 17 shows the typical waveforms observed in one experimental run using a dual-window filtering mask. Compared with the theoretical waveforms shown in Fig. 7-9, it was found that all typical waveforms similar to those theoretical ones were observed as two separated trapezoid-shaped dual peaks with a saturated maximum level (Fig. 17a), two characteristic peaks with a little superimposition (Fig. 17b), two distinguishable peaks with substantial superimposition (Fig. 17c), and an apparent one superimposed large peak (Fig. 17d). The effect of the trajectory on the waveform was also evident from the difference in the saturated peak level of two peaks as shown in Fig. 17(a).

Therefore, it is clear that the experimentally observed variations of waveforms from the radiations of the spray particles were consistent with those obtained by theoretical simulation. This result evidently proves the significant influences of the spatial distribution of particles including trajectories, offsets from the ideal image plane of the mask plane, and system design.

When a dual-window filtering mask is used for the measurement of particle parameters, all three parameters including velocity, surface temperature, and particle size can be correctly estimated only by the waveforms as shown in Fig. 17(a). Although the waveforms illustrated in Fig. 17(b) and (c) can be used to give correct velocity and a rough estimation of the surface temperature, the particle size cannot be estimated correctly. This is because the expansion of the image spot size becomes too large to allow all effective radiation from the particle to be transmitted through the masking window. As a result, the maximum

level of the signal only corresponded to the fraction of total effective radiation of the particle and Eq 8 becomes invalid. On the other hand, the accuracy of the measurement of surface temperature is difficult to ensure owing to system noise in those peak signals without the saturated maximum. With the peak shown in Fig. 17(d), the measurement of particle parameters becomes impossible because two original peaks can hardly be separated. Therefore, for a reasonable simultaneous measurement of all particle parameters, it is necessary to ensure the evolution of the trapezoid waveform with a saturated maximum level through system design and to process only those peaks in the trapezoid-shape with a saturated maximum level during subsequent data processing.

With the single-window filtering mask, the observed typical waveforms of the radiation signals from the spray particles are illustrated in Fig. 18. Generally, two typically characteristic shapes were observed that were a single peak in trapezoid shape with a saturated flat top segment and a single triangle-like peak without a flat top segment. These waveforms of the radiation signals are consistent with those expected theoretically as shown in Fig. 5 and 14. These results further prove the significant influences of the size of the image spot and the spatial distribution of spray particles.

As mentioned previously, for the triangle-like single peak, the general characteristic value of the HWFM is not related simply to particle velocity. Therefore, it cannot be applied to the estimation of particle velocity. On the other hand, the unsaturated characteristics of the maximum height in the peak do not contain the particle size information either. Therefore, the peak only in a trapezoid shape can be used to measure simultaneously the particle velocity, surface temperature, and size. The measurement of the spatial distribution of particles can also be expected with the assistance of the experimental setting technique.

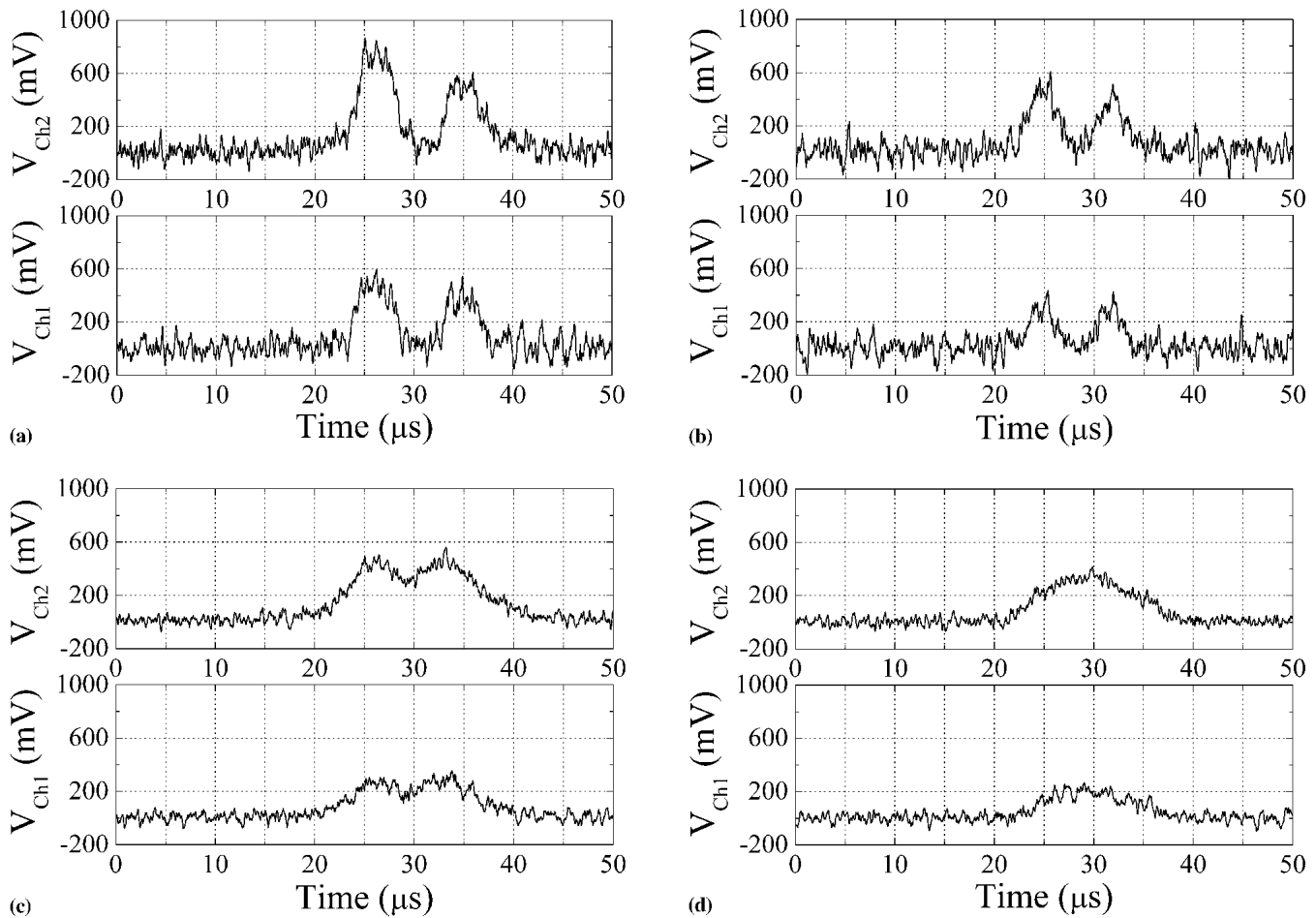


Fig. 17 Typical pulse waveforms from the radiation of in-flight particles observed with the dual-window filtering mask

**Table 1 HVOF Spraying Conditions and Measuring Settings**

Parameters		Settings
Oxygen	Pressure (MPa)	0.55
	Flow (l/min)	440
Propane	Pressure (MPa)	0.35
	Flow (l/min)	35
Powder carrier gas (N <sub>2</sub> )	Pressure (MPa)	0.35
	Flow (l/min)	10
Measuring settings	Measuring distance (mm)	60
	Aiming distance (mm)	70

As for the peak in the trapezoid shape, there are enough data to eliminate the signal noise by averaging the data in the flat segment range. Consequently, a more accurate and reliable “saturated” maximum can be obtained for the captured particle. At the same time, the post-signal processing can be simplified and rapidly performed, which is of significance for the quasi-real-time measurement.

## 6. Conclusions

1) The theoretical simulation clearly showed that the characteristic waveforms of the thermal radiation signals from

the spray particles would be varied owing to the spatial distribution of thermal spray particles around the ideal image plane of the filtering mask. The typical variations of the characteristic waveforms obtained theoretically have been observed experimentally with HVOF spraying. The waveforms expected theoretically correlated well with those observed experimentally.

- 2) The characteristic waveforms of the radiation signals from the spray particles that were trapezoid in shape with a saturated top platform contain the information of spray particle parameters including velocity, surface temperature, size, and spatial distribution. With the dual-window filtering mask, the particle velocity can be correctly measured with the bi-peak radiation signal in triangle-like shapes, and the surface temperature can be reasonably estimated. However, the particle size cannot be estimated correctly.
- 3) The waveforms of the thermal radiation signals from the spray particles were remarkably influenced by the image spot size. The waveform in a trapezoid shape can be obtained only when the image spot size is less than the width of the window on the filtering mask. A spot size larger than the width of the masking window leads to the formation of triangle-like peaks without the saturated top platform.

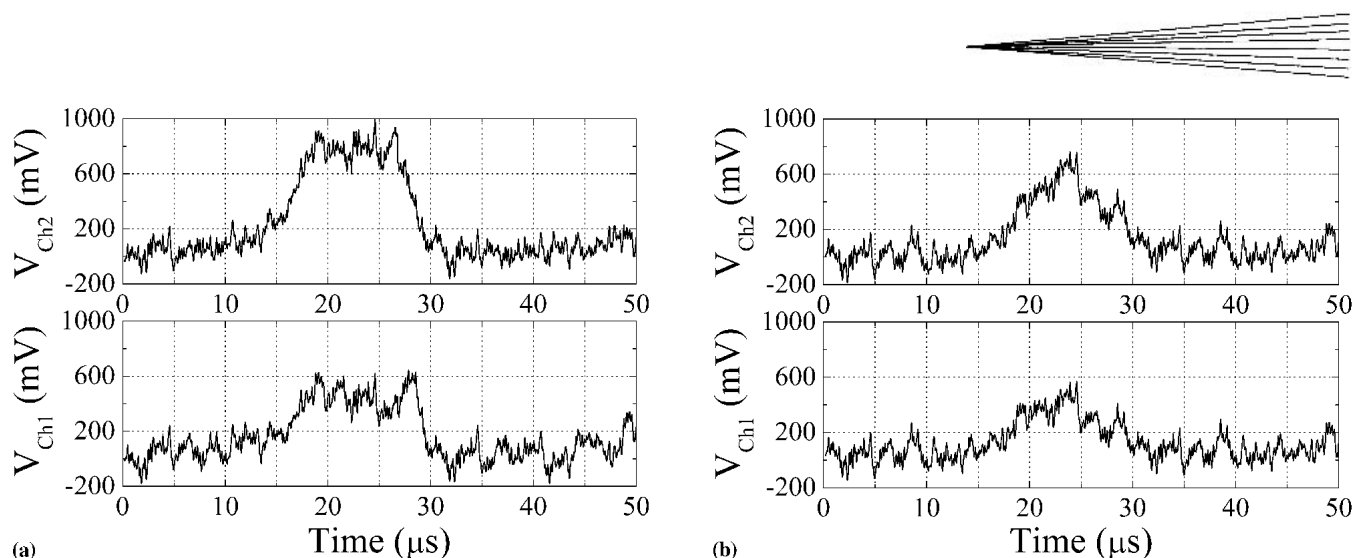


Fig. 18 Typical pulse waveforms from the radiation of in-flight particles observed with the single-window filtering mask

- 4) With the dual-window filtering mask, the characteristics of the bi-peak were significantly influenced by the interval gap between two adjacent window walls. A small interval gap leads to the significant superimposition of two characteristic peaks.
- 5) The expansion of the image spot occurs due to spatial distribution of the spray particles around the ideal image plane of the filtering mask. The effective aperture of the lens set and the offset of the particle from the ideal image plane of the filtering mask were two main factors to significantly influence the expansion of the image spot. The inclination of the particle trajectory to the axis of the lens caused the deformation of the waveform of the radiation signal from the spray particle.

### Acknowledgment

The current study was partially supported by the National Natural Science Foundation of China. (Grant No. 59401013; 59671061).

### References

1. S. Kuroda, H. Fujimori, T. Fukushima, and S. Kitahara: "Measurement of Temperature and Velocity of Thermally Sprayed Particles Using Thermal Radiation," *Trans. Japan. Welding Soc.*, 1991, 22(2), pp. 82-88.
2. A. Vardelle, M. Vardelle, R. McPherson, and P. Fauchais: "Study on Influence of Particle Temperature and Velocity Distribution Within a Plasma Jet Coating Formation" in *Proceedings of 9th International Thermal Spraying Conference, Hague, Netherlands*, 1980, pp. 30-33.
3. H.D. Steffens, K.H. Busse, and M. Schneider: "Spray Particle Behavior in a Low Pressure Plasma Jet" in *Proceedings of 11th International Thermal Spraying Conference*, Canada Welding Society, 1986, pp. 49-59.
4. L. Pawlowski: *The Science and Engineering of Thermal Spray Coatings*, John Wiley & Sons Inc., New York, NY, 1995, pp. 103-05.
5. V.P. Lyagushkin and O.P. Solonenko: "A Method to Simultaneously Measure the Velocity and Temperature of Disperse Particles in High Temperature Flow" in *Proceedings of 7th International Conference on Plasma Chemistry*, Eindhoven, Netherlands, Vol. 2, 1985, pp. 730-35.
6. C. Moreau, P. Gougeon, M. Lamontagne, V. Lacasse, G. Vaudreuil, and P. Cielo: "On-Line Control of the Plasma Spraying Process by Monitoring the Temperature, Velocity and Trajectory of In-Flight Particles" in *Thermal Spray Industrial Applications*, C. C. Berndt and S. Sampath, ed., ASM International, Materials Park, OH, 1994, pp. 431-37.
7. L. Leblanc, P. Gougeon, and C. Moreau: "Investigation of the Long-Term Stability of Plasma Spraying by Monitoring Characteristics of the Spray Particles" in *Thermal Spray: A United Forum for Scientific and Technological Advances*, C.C. Berndt, ed., ASM International, Materials Park, OH, 1997, pp. 567-75.
8. M.P. Planche, R. Bolot, O. Landemarre, and C. Coddet: "Comparison Between Experimental and Numerical Results Obtained on In-Flight Particles Characteristics" in *Thermal Spray: Meeting the Challenges of the 21st Century*, C. Coddet, ed., ASM International, Materials Park, OH, 1998, pp. 355-60.
9. M. Schutz, G. Barbezat, and E. Fluck: "Measurement Technology for In-Flight Particle Diagnosis in Plasma Spraying" in *Thermal Spray: Meeting the Challenges of the 21st Century*, C. Coddet, ed., ASM International, Materials Park, OH, 1998, pp. 761-66.
10. L. Leblanc and C. Moreau: "In-Flight Particle Characteristics of Plasma-Sprayed Dense Yttria Stabilized Zirconia" in *Thermal Spray: Meeting the Challenges of the 21st Century*, C. Coddet, ed., ASM International, Materials Park, OH, 1998, pp. 773-78.
11. L. Leblanc, C. Moreau, P. Gougeon and J. Xi: "Long-Term Stability of Plasma Spraying: Study on the Evolution of the In-Flight Particle State, Coating Microstructure, Voltage and Acoustic Signatures" in *Tagungsband Conference Proceedings (Proceedings of United Thermal Spray Conference, 1999)*, E. Lugscheider and R.A. Kammer, ed., DVS—German Welding Society, Germany, 1999, pp. 306-11.
12. L. Leblanc, C. Moreau, J-G. Legoux, and B. Arsenaud: "Characterization of Plasma Spray Processes by Monitoring the State of the Sprayed Particles" in *Tagungsband Conference Proceedings (Proceedings of United Thermal Spray Conference, 1999)*, E. Lugscheider and R.A. Kammer, ed., DVS—German Welding Society, Germany, 1999, pp. 329-34.
13. D.L. Gilmore, R.A. Neiser, Y. Wan, and S. Sampath: "Process Maps for Plasma Spray" in *Part 1: Plasma-Particle Interaction, Thermal Spray: Surface Engineering via Applied Research*, C.C. Berndt, ed., ASM International, Materials Park, OH, 2000, pp. 149-55.
14. S. Kuroda, Y. Tashiro, H. Yumoto, S. Taira, and H. Fukunuma: "Peening Action and Residual Stresses in HVOF Thermal Spraying of 316L Stainless Steel" in *Thermal Spray: Meeting the Challenges of the 21st Century*, C. Coddet, ed., ASM International, Materials Park, OH, pp. 569-74.
15. E. Lugscheider, C. Herbst, A. Fischer, and L. Zhao: "Influence of HVOF Process Parameters on Particle Parameters During Spraying of Metal Alloy" in *Tagungsband Conference Proceedings (Proceedings of United Thermal Spray Conference, 1999)*, E. Lugscheider and R.A. Kammer, ed., DVS—German Welding Society, Germany, 1999, pp. 428-33.
16. L. Jacobs, M.M. Hyland, J. Gutleber, and S. Sampath: "Study of the Decarburization Reactions and Phase Transformations of a WC-Co

- Powder” in *Tagungsband Conference Proceedings (Proceedings of United Thermal Spray Conference, 1999)*, E. Lugscheider and R.A. Kammer, ed., DVS—German Welding Society, Germany, 1999, pp. 439-45.
17. R. Benary: “A Study and Comparison of Spray Stream Formation Using Two Wire Arc 90-Degree, and 0-Degree Spray Processes” in *Tagungsband Conference Proceedings (Proceedings of United Thermal Spray Conference, 1999)*, E. Lugscheider and R.A. Kammer, ed., DVS — German Welding Society, Germany, 1999, pp. 242-46.
  18. E. Lugscheider, C. Herbst-Dederichs, and L. Zhao: “Particle Behavior in a Powder-Laden HVOF Jet” in *Thermal Spray: Surface Engineering via Applied Research*, C.C. Berndt, ed., ASM International, Materials Park, OH, 2000, pp. 501-08.
  19. G. Bourque, M. Lamontagne, and C. Moreau: “A New Sensor for On-line Monitoring the Temperature and Velocity of Thermal Spray Particles” in *Thermal Spray: Surface Engineering via Applied Research*, C.C. Berndt, ed., ASM International, Materials Park, OH, 2000, pp. 45-50.
  20. L. Pouliot, J. Blain, F. Nadeau, M. Lamontagne, J.F. Bisson, and C. Moreau: Significant Increase in the Sensitivity of In-Flight Particle Detector Through Improvements and Innovation” in *Thermal Spray 2001: New Surfaces for a New Millennium*, C.C. Berndt, K.A. Khor, and E. Lugscheider, ed., ASM International, Materials Park, OH, 2001, pp. 723-26.
  21. T.D. McGee: *Principles and Methods of Temperature Measurement*, John Wiley & Sons Inc., New York, NY, 1988, pp. 353-72.
  22. D.P. DeWitt and G.D. Nutter: *Theory and Practice of Radiation Thermometry*, John Wiley & Sons Inc., New York, NY, 1988, pp. 21-63.